JOURNAL OF AIRCRAFT
Vol. 46, No. 5, September–October 2009

Engineering Notes

Flight Dynamics of High-Aspect-Ratio Flying Wings: Effect of Large Trim Deformation

Brijesh Raghavan* and Mayuresh J. Patil†
Virginia Polytechnic Institute and State University,
Blacksburg, Virginia 24061-0203

DOI: 10.2514/1.36847

I. Introduction

PATIL and Hodges [1] presented an integrated model for the aeroelasticity and flight dynamics of a high-aspect-ratio flying wing. The authors conducted a nonlinear trim computation for straight and level trim flight and compared the results for a flexible configuration and the corresponding rigid configuration based on the undeformed shape before application of loads. The nonlinear model was linearized about the trim point and eigenvalues were computed to study the linear stability characteristics of the airplane at the trim point. A root-locus plot for the longitudinal flight dynamic eigenvalues was generated with the payload at the center as the variable for both the rigid body based on the undeformed shape and the flexible configuration. Results showed that the root-locus plot for the rigid body configuration did not capture the trend shown by the flexible configuration.

This paper uses the integrated model developed by Patil and Hodges [1] to understand the effect of nonlinear static aeroelastic deformation on the flight-aeroelastic stability of a flexible flying wing configuration. Additional trim cases and lateral flight dynamic characteristics not studied by Patil and Hodges [1] are also presented here. Trim results are presented for climbing flight, level turn, and climbing turn. Linear stability analysis is carried out about straight and level trim and root-locus plots for longitudinal and lateral flight dynamic modes are compared for three configurations: the flexible configuration, a rigid body configuration based on the deformed shape at trim, and a rigid body configuration based on the undeformed shape before trim.

II. Mathematical Modeling

The integrated modeling for the aeroelasticity and flight dynamics of a flexible, high-aspect-ratio flying wing has been published previously [1,2] and will not be repeated here. To trim the airplane in turning flight, a few additions were made to the control allocation and the mathematical modeling which are presented next.

As in [1], the flying wing configuration used in this paper has five engines evenly spaced along the wing span as shown in Fig. 1. The entire trailing edge is actuated and is split into two sections along the span. The two sections deflect in the same direction for pitch control and differentially for roll control. The total control surface deflection for each section is calculated by adding up these two components. As the flying wing does not have a rudder or vertical tail, yaw control is obtained by linearly redistributing thrust across the different engines. The differential thrust ΔT is chosen such that it is zero at the center and changes by integral multiples across the wingspan.

The trim state of the system is specified in terms of the flight speed V_∞, the flight path angle γ, and the rate of turn in the inertial frame r_i. Sideslip is constrained to be zero. The corresponding equations for specifying these quantities are given by

$$|\mathbf{V}^{n_g}|^2 - V_\infty^2 = 0 \tag{1}$$

$$\boldsymbol{\Omega}^{n_g}.(\mathbf{g}^{n_g}/g_0) - r_i = 0 \tag{2}$$

$$\mathbf{V}^{n_g}.(\mathbf{g}^{n_g}/g_0) + V_\infty \sin\gamma = 0 \tag{3}$$

$$V_1^{n_g} = 0 \tag{4}$$

where n_g refers to the reference node at the center of the wing, g_0 is the magnitude of acceleration due to gravity, $\mathbf{V}$, $\boldsymbol{\Omega}$, and $\mathbf{g}$ are velocity, angular velocity, and gravitational vectors, respectively, and V_1 is the velocity component along the local X axis.

The set of equations presented in [1] along with the four constraint equations given previously constitute a set of nonlinear equations in terms of the structural states, unsteady aerodynamic states, and trim control values (thrust, flap deflection, aileron deflection, differential thrust). These nonlinear equations are solved using the Newton–Raphson method to compute the trim configuration as well as the thrust T, flap δ_f, aileron deflection δ_a, and the differential thrust ΔT. Following trim computation, the equations are linearized at the trim point. Linear stability analysis is carried out by computing the eigenvalues of the linearized system. These eigenvalues indicate the stability of the system for small perturbations about the trim point.

III. Results

A. Verification

Though the mathematical modeling used in this paper is based on previously published work[1], the code used to generate these results is a new implementation that was developed as part of a closed-loop system for path following [3]. The open-loop aeroelastic code has been verified for a number of test cases against standard results. Boundary conditions are changed to simulate a cantilevered beam case by specifying the velocity, angular velocity, and pitch angle at the root. Flutter prediction results from the code are compared with results from an analytical model for the Goland wing [4,5] for which the parameters are given in Tables 1 and 2. Free-vibration bending frequencies, Euler buckling loads, divergence velocity, and control reversal velocity are compared with analytical results for a modified Goland wing, which has its sectional center of mass relocated to the

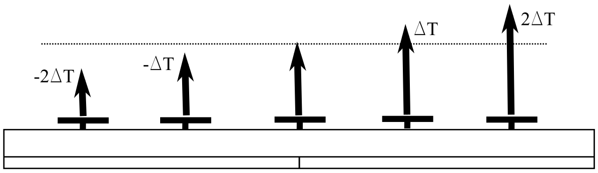

Fig. 1 Differential thrust.

Presented as Paper 6383 at the AIAA Atmospheric Flight Mechanics Conference and Exhibit, Hilton Head, South Carolina, 20–23 August 2007; received 25 January 2008; revision received 7 May 2009; accepted for publication 8 May 2009.

*Graduate Student, Department of Aerospace and Ocean Engineering; brijeshr@vt.edu. Student Member AIAA.

†Assistant Professor, Department of Aerospace and Ocean Engineering; mpatil@vt.edu. Senior Member AIAA.

Table 1 Geometric parameters for Goland wing

$b = 6.096$ m	$C_{L_0} = 0$	$C_{L_\alpha} = 2\pi$	$C_{L_\delta} = 1$	$C_{D_0} = 0.0$
$c = 1.829$ m	$C_{m_0} = 0$	$C_{m_\alpha} = 0$	$C_{m_\delta} = -0.25$	$\mu = 35.71$ kg/m
	$I_{xx} = 8.641$ kg · m	$I_{yy} = 0.0$ kg · m	$I_{zz} = 8.641$ kg · m	

Table 2 Elastic parameters for Goland wing

No. of nodes	41
Sectional center of gravity	43% chord
Elastic axis position	33% chord
Torsional rigidity	0.987×10^6 N · m^2
Bending rigidity	9.77×10^6 N · m^2

beam elastic axis. These results are presented in Table 3. Application of a sufficiently large moment about the Y axis at the tip of the beam is seen to deform the beam into a circle as shown in Fig. 2, thus verifying geometric exactness of the beam model.

Figure 3 plots the log of the percentage error between the computed and analytical bending frequencies for the cantilevered beam versus the log of the number of the nodes. The plots for all three modes show a slope of negative 2. This implies that the percentage error in the computed frequency decreases with an increase in number of nodes, and that the percentage error is inversely proportional to the square of the number of nodes.

B. Sample Configuration

The configuration used in this paper is identical to the one studied in [1] except for the following two features. The three landing gear pods have been eliminated and the location of the sectional mass has been moved to 22% chord. Parametric values used to define the configuration are given in Tables 4 and 5. A schematic of the configuration is given in Fig. 4.

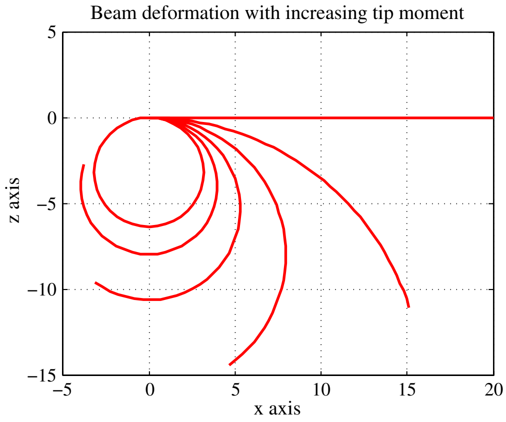

Fig. 2 Test for geometric exactness.

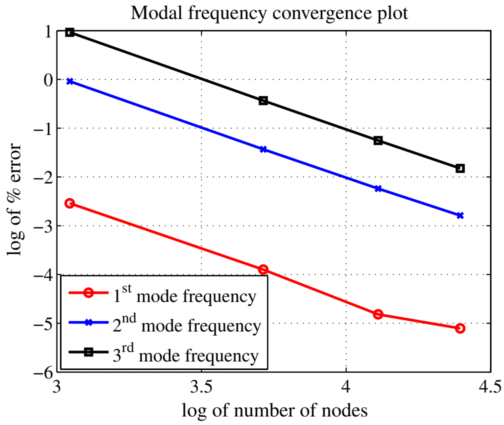

Fig. 3 Error convergence plot for bending frequencies.

To identify the influence of static aeroelastic deformation on the open-loop flight dynamics, the following three configurations are compared: an undeformed rigid flying wing ("undeformed"), a rigid flying wing defined using static aeroelastic deformation at trim for a given flight condition ("deformed"), and a flexible flying wing configuration ("flexible"). The analysis is carried out in two steps: trim computation, followed by linear stability analysis.

C. Trim Computation

A comparison of control parameters at straight and level trim for the undeformed and flexible configurations was carried out by Patil and Hodges [1], and has not been repeated here. This section presents control parameters computed for four different trim states for the flexible/deformed configuration. The trim computed for the flexible configuration is used to defined the rigid body shape for the deformed configuration.

Figures 5–7 show the variation of control parameters with nodal mass at the center (payload) for four different trim cases. These consist of a straight and level trim at 12.19 m/s at sea level, a straight climb at 12.19 m/s at a 2 deg slope, a level turn at 12.19 m/s with a radius of 6096 m, and a helical climbing turn at 12.19 m/s with a 2 deg slope and a radius of 6096 m. Increasing the payload mass at the center increases the net bending moment acting on the wing, leading to a larger bending deformation and a corresponding decrease in local angle of attack on the outboard wing sections. This effect is reflected in the variation of the required angle of attack at the root and the required aileron deflection with increasing payload mass.

As previously observed in [1], the variation in thrust required for straight and level trim is not found to vary significantly with the payload mass. This is attributed to the fact that the 2-D aerodynamic model assumes a constant C_{D_0}. The thrust required for climbing flight with a 2-deg flight path angle increases linearly with nodal mass. This is consistent with the aircraft performance equation which shows that excess thrust required for climb increases linearly with aircraft weight for a given flight path angle [6]. The required flap deflection is positive at low values of payload mass. This value decreases with increasing payload mass and becomes negative. The decrease and change in sign of the required flap deflection can be attributed to the increase in the pitch-down moment created by the outboard engines with increasing bending deformation.

The angle of attack at the center node at trim is seen to increase monotonically for all trim cases. This can be attributed to the decrease in the contribution of the outboard wing sections to net aerodynamic force in the vertical direction with increasing bending deformation.

The magnitude of the required aileron deflection increases with increasing payload mass. Once again, this can be attributed to the decrease in aileron effectiveness of the outboard section of the wing with increasing bending deformation. Neither the deformation, nor the sectional aerodynamic forces and moments are symmetric about the body frame YZ plane for a flying wing trimmed in turning flight, resulting in an aerodynamic yawing moment. The differential thrust ΔT gets adjusted accordingly to trim the airplane with zero sideslip.

D. Linear Stability Analysis for Straight and Level Trim

This section looks at the variation of the Dutch roll, the phugoid, and the spiral eigenvalues with the nodal mass at the center of the flying wing. The root-locus plots for the eigenvalues are obtained by varying the nodal mass from 0 to 249.47 kg. The eigenvalues corresponding to the 0 kg case are indicated by squares on the root-locus plots, whereas the eigenvalues corresponding to the 249.47 kg

Table 3 Verification results

		Analytical	Computational	Percentage difference
Flutter	Velocity	137.16 m/s	136.22 m/s	0.68%
	Frequency	70.685 rad/s	70.063 rad/s	0.88%
Free-vibration bending frequencies	First mode	49.492 rad/s	49.502 rad/s	0.02%
	Second mode	310.16 rad/s	310.90 rad/s	0.24%
	Third mode	868.46 rad/s	874.07 rad/s	0.65%
Divergence velocity		252.39 m/s	250.82 m/s	0.62%
Control reversal velocity		141.38 m/s	141.40 m/s	0.01%
Euler buckling load		648.93 kN	649.10 kN	0.03%
Tip moment for circle		100.73 kNm	100.94 kNm	0.002%

Table 4 Geometric parameters for the sample configuration

$b = 73.06$ m	$C_{L_0} = 0$	$C_{L_\alpha} = 2\pi$	$C_{L_\delta} = 1$	$C_{D_0} = 0.01$
$c = 2.44$ m	$C_{m_0} = 0.025$	$C_{m_\alpha} = 0$	$C_{m_\delta} = -0.25$	$\mu = 8.93$ kg/m
	$I_{xx} = 4.15$ kg · m	$I_{yy} = 0.69$ kg · m	$I_{zz} = 3.46$ kg · m	

Table 5 Elastic parameters for the sample configuration

No. of nodes	25
Payload mass variation at center	0–250 kg
Wing tip dihedral	5 deg
Position of wing tip dihedral	12.19 m from wing tip
Sectional center of gravity	22% chord
Elastic axis position	25% chord
Torsional rigidity	0.165×10^6 N · m^2
Bending rigidity	1.03×10^6 N · m^2
Bending rigidity (*chordwise*)	12.39×10^6 N · m^2

case are indicated by triangles. The roll mode and short period mode couple with the unsteady aerodynamic modes in the undeformed and deformed configuration and with the aeroelastic modes in the flexible configuration and are not studied in this section. The Dutch roll and the phugoid mode exhibit dynamic instability as the nodal mass at the center of the wing is increased. This onset of dynamic instability in

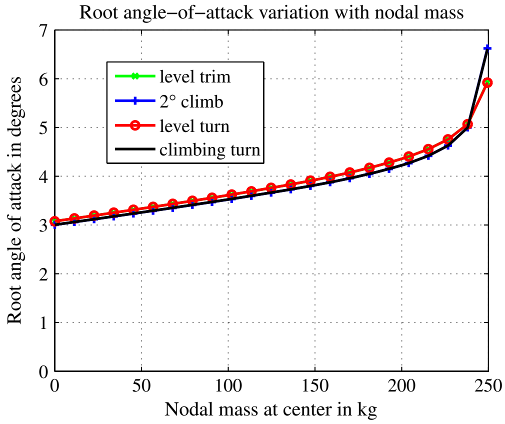

Angle of attack at trim

Fig. 6 Trim parameters.

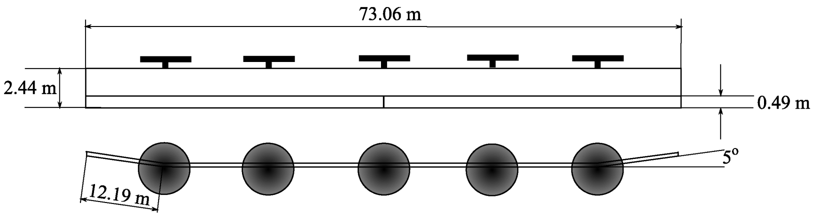

Fig. 4 Schematic of configuration.

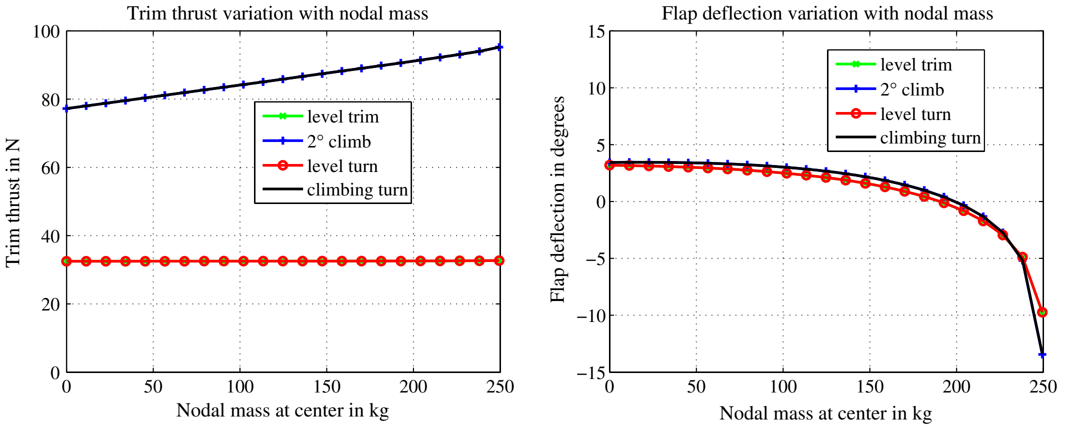

a) Trim thrust **b) Flap deflection at trim**

Fig. 5 Trim parameters.

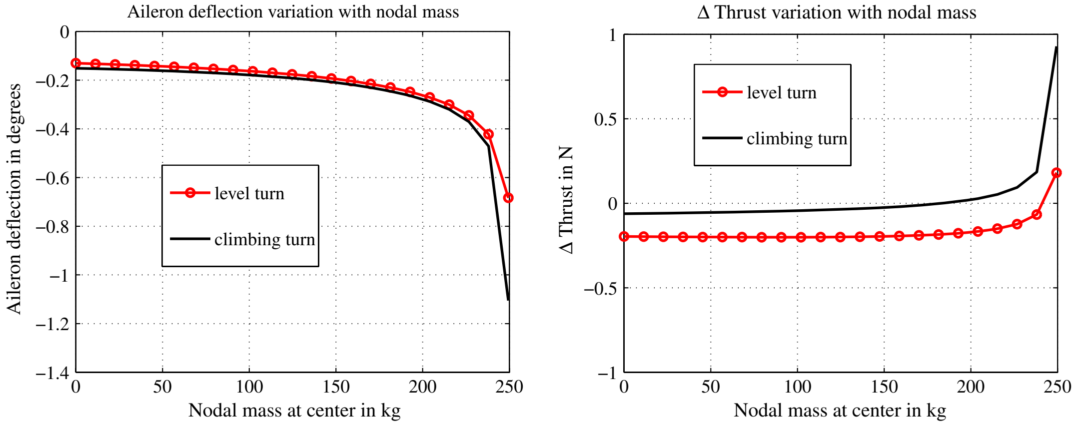

a) Aileron deflection at trim

b) ΔThrust at trim

Fig. 7 Trim parameters.

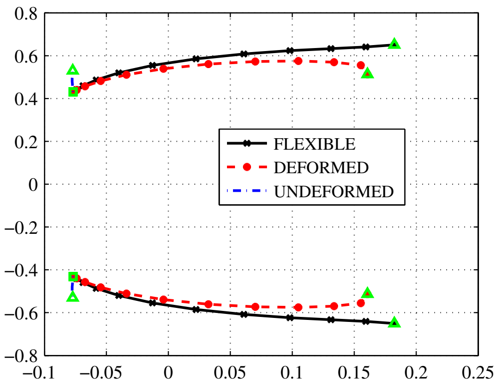

Fig. 8 Root-locus plot for phugoid.

the flexible configuration is captured by the deformed configuration but not by the undeformed configuration.

The root-locus plot for the phugoid mode is shown in Fig. 8. For both the flexible and deformed configuration, the phugoid mode is seen to go unstable with increasing payload mass, though the undeformed configuration remains stable as seen in Fig. 8. More significantly, the phugoid mode corresponding to the flexible configuration goes unstable near the mass value at which the phugoid mode of the deformed configuration crosses the zero damping line. Table 6 shows eigenvalues for phugoid modes for two values of payload, denoted by “light” (45.35 kg) and “heavy” (181.4 kg), respectively.

The root-locus plot for lateral–directional modes is plotted in Fig. 9. For lateral–directional modes, the eigenvalues of the deformed configuration are close to those of the flexible configuration. The Dutch roll mode is seen to go unstable with increasing payload mass (Fig. 9b). Once again, it is seen that the instability in the Dutch roll mode in the flexible configuration is captured by the deformed configuration, but not by the undeformed configuration. The spiral mode is seen to be stable for the entire range of nodal mass for all three configurations. Table 7 shows eigenvalues for lateral–directional modes for the light and heavy payload cases.

E. Stability Boundary for Straight and Level Trim

For a flying wing trimmed in straight and level flight, Fig. 10 shows the dependence of stability on the payload mass at the center node and position of chordwise sectional center-of-gravity location. In the graph, the vertical line corresponds to the static stability boundary of the flying wing, and the horizontal line corresponds to the dynamic stability boundary. The deformed rigid wing is seen to go dynamically unstable at a lower payload value than the corresponding flexible system for all chordwise positions of center of gravity. For both configurations, the Dutch roll mode is the one that goes dynamically unstable at a lower payload (as compared to the phugoid mode) for the entire center-of-gravity range.

A two-dimensional airfoil has its aerodynamic center at the quarter-chord point and shows static stability when the center of gravity is located ahead of this point. The static stability boundary for the two-dimensional airfoil case corresponds to a vertical line at an x coordinate value of zero in Fig. 10. However, the static stability boundary for the flying wing is not seen to be a vertical line in Fig. 10. This can be attributed to the static aeroelastic deformation of the configuration at trim. For configurations which undergo significant structural deformation or have engines vertically offset from the center of gravity, thrust does induce a pitching moment. In this case,

Table 6 Longitudinal eigenvalues

		Light payload (45.35 kg)	Heavy payload (181.4 kg)
Undeformed	Phugoid	$-0.0773 \pm 0.4509i$	$-0.0775 \pm 0.5052i$
Deformed	Phugoid	$-0.0672 \pm 0.4572i$	$0.1049 \pm 0.5754i$
Flexible	Phugoid	$-0.0689 \pm 0.4596i$	$0.0981 \pm 0.6235i$

Table 7 Lateral–directional eigenvalues

		Light payload (45.35 kg)	Heavy payload (181.4 kg)
Undeformed	Dutch roll	$-0.0045 \pm 0.1410i$	$-0.0043 \pm 0.1410i$
	Spiral	-0.1559	-0.2060
Deformed	Dutch roll	$-0.0016 \pm 0.2003i$	$4.2488e - 005 \pm 0.3499i$
	Spiral	-0.1587	-0.2392
Flexible	Dutch roll	$-0.0028 \pm 0.1987i$	$0.0044 \pm 0.3654i$
	Spiral	-0.1925	-0.2616

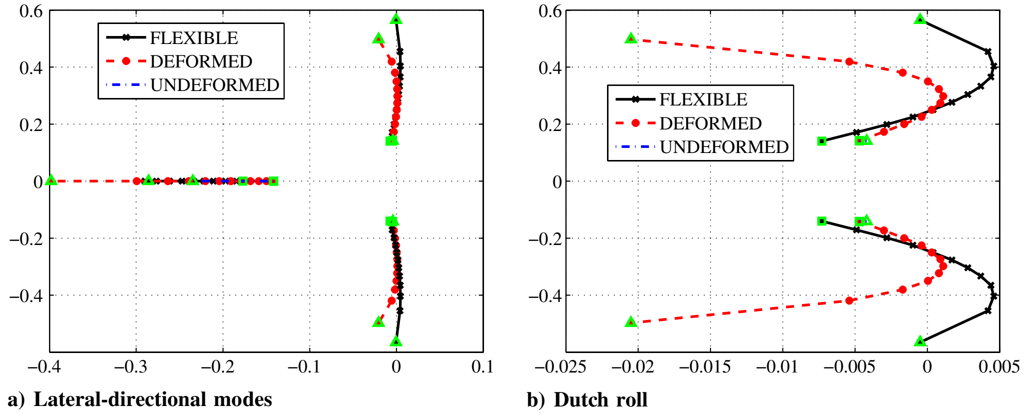

a) Lateral-directional modes b) Dutch roll

Fig. 9 Root-locus plot for lateral–directional mode.

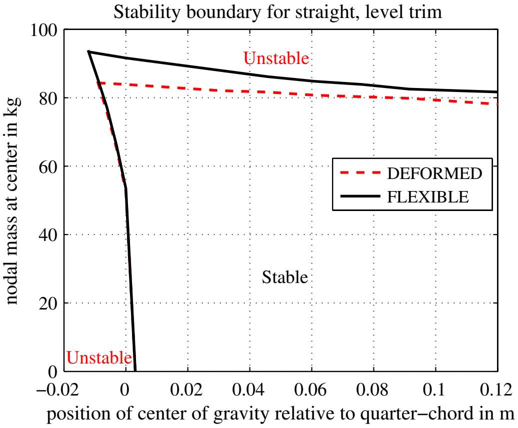

Fig. 10 Stability boundary.

the aerodynamic pitching moment at trim about the center of gravity is nonzero. The condition for static stability gets modified as

$$(C_{m_\alpha}^{\text{aero}})_{\text{cg}} - (C_m^{\text{aero}})_{\text{cg}} \frac{C_{L_\alpha}}{C_L} < 0 \qquad (5)$$

where $(C_m^{\text{aero}})_{\text{cg}}$ is the nondimensional aerodynamic pitching moment coefficient about the center of gravity, C_L is the nondimensional lift coefficient, and the subscript α refers to the slope of the graph when $(C_m^{\text{aero}})_{\text{cg}}$ or C_L is plotted against the angle of attack.

The above condition can be obtained by assuming a nonzero aerodynamic pitching moment at trim, and computing the determinant of the coefficients of the four linearized equations for dynamics in the longitudinal plane. For a given chordwise center-of-mass location, the criteria obtained in Eq. (5) are found to predict the nodal mass value for the onset of static instability for the deformed configuration with an error of less than 1% and for the flexible configuration with an error of 2%.

IV. Conclusions

This paper presented various trim cases and lateral flight dynamic characteristics for a flexible high-aspect-ratio flying wing configuration. Trim results were presented for climb, level turn, and climbing turns. The integrated nonlinear model of the aeroelasticity and flight dynamics was linearized at straight and level trim and linear stability analysis was carried out. It is seen that the root-locus plot of the flight dynamic eigenvalues of the deformed configuration track those of the flexible configuration, whereas those of the undeformed configuration do not. For a given chordwise center-of-gravity location, the Dutch roll mode is the first one to go unstable with increasing payload mass, for both the statically deformed and the flexible configuration. For a high-aspect-ratio flying wing configuration, static aeroelastic deformation is shown to account for the predominant discrepancy between the flight dynamic characteristics at trim predicted using a flexible model, and the flight dynamic characteristics predicted using a rigid body model. Thus, one may use a rigid body flight dynamic model based on the trim shape (accounting for static aeroelastic deformation) to conduct preliminary design and control synthesis.

References

[1] Patil, M. J., and Hodges, D. H., "Flight Dynamics of Highly Flexible Flying Wings," *Journal of Aircraft*, Vol. 43, No. 6, Nov.–Dec. 2006, pp. 1790–1798.
doi:10.2514/1.17640

[2] Chang, C.-S., Hodges, D. H., and Patil, M. J., "Aeroelastic Characteristics of a Highly Flexible Aircraft," *Journal of Aircraft*, Vol. 45, No. 2, March–April 2008, pp. 538–545.

[3] Raghavan, B., and Patil, M. J., "Flight Control for Flexible High Aspect-Ratio Flying Wing," *International Forum on Aeroelasticity and Structural Dynamics*, IFASD-2009-068, June 2009.

[4] Goland, M., "The Flutter of a Uniform Cantilever Wing," *Journal of Applied Mechanics*, Vol. 12, No. 4, 1945, pp. A197–A208.

[5] Goland, M., and Luke, Y., "The Flutter of a Uniform Cantilever Wing with Tip Weights," *Journal of Applied Mechanics*, Vol. 15, No. 1, 1948, pp. 13–20.

[6] Anderson, J. D., Jr., *Aircraft Performance and Design*, McGraw–Hill, New York, 1999, p. 265.